

# Peer-Reviewed Technical Communication

## Mitigation of Intercarrier Interference for OFDM Over Time-Varying Underwater Acoustic Channels

Kai Tu, Dario Fertonani, Tolga M. Duman, *Fellow, IEEE*, Milica Stojanovic, *Fellow, IEEE*, John G. Proakis, *Life Fellow, IEEE*, and Paul Hursky, *Member, IEEE*

**Abstract**—Orthogonal frequency division multiplexing (OFDM) has emerged as a promising modulation scheme for underwater acoustic (UWA) communications, thanks to its robustness to channels with severe time dispersion. Compared to conventional single-carrier systems, for which complicated equalization schemes are usually required, OFDM systems are in general much simpler to implement as detection can be carried out symbol-by-symbol over time-dispersive channels. In this paper, we focus on cyclic-prefixed OFDM over time-varying UWA channels. To cope with the intercarrier interference (ICI) that arises at the receiver side because of the time variations in the channel, we consider two ICI-mitigation techniques. In the first scheme, the ICI coefficients are explicitly estimated, and minimum mean square error linear equalization based on such estimates is performed. In the second approach, no explicit ICI estimation is performed, and detection is based on an adaptive decision-feedback equalizer applied in the frequency domain across adjacent subcarriers. To cope with the phase variations of the ICI coefficients, phase-tracking loops are introduced in both ICI-mitigation schemes. The effectiveness of the presented schemes is demonstrated through simulation results, as well as real data collected in a recent experiment conducted in shallow water off the western coast of Kauai, HI, in June 2008.

**Index Terms**—Frequency-domain equalization, intercarrier interference (ICI) mitigation, orthogonal frequency division multiplexing (OFDM), underwater acoustic (UWA) communications, wideband Doppler effect.

### I. INTRODUCTION

UNDERWATER ACOUSTIC (UWA) channels are generally considered as one of the most challenging communication media, mainly because of their high time-frequency selectivity [1]. Compared to terrestrial radio channels, shallow-water UWA channels typically exhibit a much greater

time dispersion, even on the order of hundreds of milliseconds [1]. In classical single-carrier communication systems, such multipath spreads cause severe intersymbol interference (ISI), which requires sophisticated and computationally demanding equalization techniques. Transmission schemes based on orthogonal frequency division multiplexing (OFDM) have recently emerged as an attractive solution for UWA communications [2]–[6]. For example, promising results have been obtained in a recent UWA communication experiment, AU-Vfest07, performed in June 2007 off the coast of Panama City, where an OFDM-based scheme was able to provide reliable communications at horizontal distances up to 3500 m, with rates up to 50 kb/s [6].

The key advantage provided by OFDM transmissions is that, for time-invariant channels, modulation symbols transmitted over different subcarriers do not interfere with each other even after propagating over frequency-selective channels, so that simple symbol-by-symbol detection can be adopted [2]. Unfortunately, this property no longer holds on time-varying channels, as intercarrier interference (ICI) arises [7]–[11]. In wireless radio communications, the time variations are typically very small with respect to the duration of the OFDM symbols; therefore, satisfactory detection performance can be achieved even if ICI is neglected. For example, the ICI due to the Doppler effect can safely be neglected in most wireless channels, since the relative speed between the transmitter and the receiver is usually several orders of magnitude lower than the speed of light (e.g., seven orders of magnitude for a relative speed of 100 km/h). On the contrary, the speed of sound in water is about 1.5 km/s, hence even relative speeds of a few meters per second may cause significant ICI.

Techniques for Doppler shift estimation and compensation can be found in [4], [5], where it is also shown that in many cases no significant ICI is present after proper compensation of the Doppler shift. Here, we focus on more challenging UWA environments, where the Doppler shift is not the only significant source of ICI. Most of the existing ICI-mitigation schemes are based on a two-step approach: first, an estimate of the ICI coefficients is obtained; then a suitable ICI-mitigation technique exploiting such estimates is employed. For these approaches, the most critical part appears to be estimation of the ICI coefficients, which generally exploits pilot symbols in the transmitted sequence [7], [9], [11], [12]. Several ICI-mitigation schemes exploiting the basis expansion model (BEM) [13] have been proposed [8], [14]–[18]. However, it was shown in [19] that various

Manuscript received July 29, 2009; revised April 29, 2010, September 01, 2010; accepted February 28, 2011. Date of publication May 12, 2011; date of current version May 27, 2011. This work was funded by the multidisciplinary university research initiative (MURI) Grants N00014-07-1-0738/0739. This paper was presented in part at *IEEE Oceans 2009*, Bremen, Germany, May 2009.

**Associate Editor:** U. Mitra.

K. Tu, D. Fertonani, and T. M. Duman are with the School of Electrical, Computer and Energy Engineering, Arizona State University, Tempe, AZ 85287-5706 USA (e-mail: duman@asu.edu).

M. Stojanovic is with the Department of Electrical and Computer Engineering, Northeastern University, Boston, MA 02115 USA.

J. G. Proakis is with the Department of Electrical and Computer Engineering, University of California, San Diego, La Jolla, CA 92093 USA.

P. Hursky is with the HLS Research, Inc., La Jolla, CA 92037 USA.

Color versions of one or more of the figures in this paper are available online at <http://ieeexplore.ieee.org>.

Digital Object Identifier 10.1109/JOE.2011.2123530

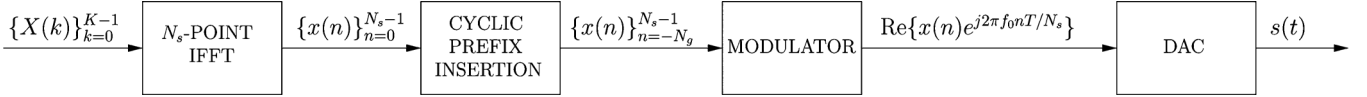


Fig. 1. Block diagram of a CP-OFDM transmitter.

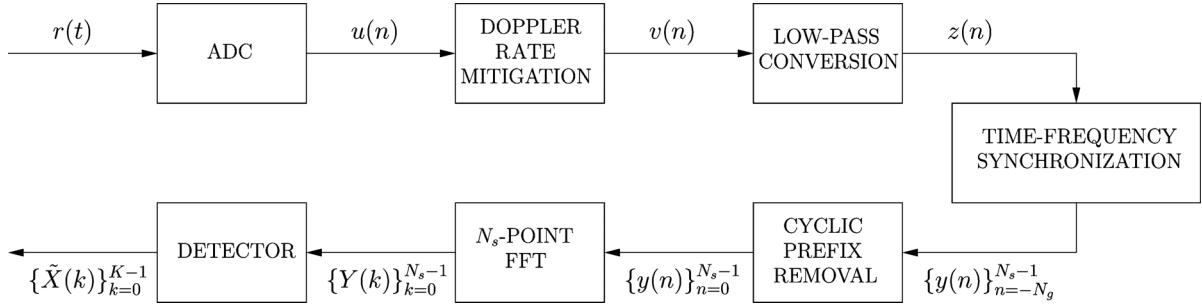


Fig. 2. Block diagram of the considered receiver.

cases exist where BEM-based ICI mitigation is outperformed even by the standard ICI-neglecting receivers. A promising alternative consists of explicitly modeling the channel variations and exploiting the model in the receiver design (for example, see [20]). Some algorithms, such as the one presented in [9], rely on the wide sense stationary uncorrelated scattering (WSSUS) assumption for the channel model, which may be acceptable for most wireless radio channels, but is unlikely to be satisfied in UWA channels [1]. Some algorithms, such as the one presented in [21], rely on pilot symbols with a very particular structure. In all these cases, the frequency-domain equalization performed by the ICI-mitigation techniques is computationally much simpler than the time-domain equalization that would be required for single-carrier communications over the same channel [7]–[11].

In this paper, we consider two ICI-mitigation techniques that do not rely on any particular assumption on the channel statistics, nor on the structure of the pilot symbols. In the first scheme, the ICI coefficients are estimated by means of a closed-loop tracking system, based on which minimum mean square error (MMSE) linear equalization [22] is performed in the frequency domain. In the second scheme, no explicit ICI estimation is performed, and detection is made by means of an adaptive decision-feedback equalizer (DFE) [22] in the frequency domain. To cope with the phase variations of the ICI coefficients, phase-tracking schemes are introduced in both cases. We present simulation results showing that the considered schemes can provide significant performance improvements with respect to the standard receivers that neglect the ICI. We also discuss decoding of UWA-communication data recorded in the Kauai Acomms MURI 2008 (KAM08) experiment [23], which was conducted in shallow water off the western coast of Kauai, HI, in June 2008. Particularly, we present results for a 4-km link with no motion between the transmitter and the receiver, and a 2-km link in which the transmitting transducer was towed at a speed of 3 knots.

The paper is organized as follows. Section II introduces the system model for OFDM transmissions over time-varying UWA channels and describes the pre-detection synchronization stage. In Section III, we discuss different detection schemes, with and without ICI mitigation. In Section IV, we present numerical re-

sults for simulated channels as well as results obtained in the KAM08 experiment, comparing the performance of the considered detection schemes. Finally, Section V provides some concluding remarks.

## II. SYSTEM MODEL

An OFDM system with  $K$  subcarriers is considered, where  $K$  is an integer power of two. An OFDM frame consists of  $K$  symbols  $\{X(k)\}_{k=0}^{K-1}$ , obtained by mapping a sequence of (possibly channel-coded and interleaved) bits into a suitable complex-valued constellation, such as phase-shift keying (PSK) or quadrature amplitude modulation (QAM). A subset of the  $K$  symbols are typically used as pilot symbols, to be exploited for channel estimation at the receiver side. The continuous-time OFDM waveform  $s(t)$  is obtained by modulating the symbols  $\{X(k)\}_{k=0}^{K-1}$  over a set of orthogonal subcarriers, as follows:

$$s(t) = \text{Re} \left\{ \sum_{k=0}^{K-1} X(k) e^{j2\pi f_k t} \right\}, \quad t \in \{-T_g, T\} \quad (1)$$

where  $f_k = f_0 + k/T$  is the frequency of the  $k$ th subcarrier,  $1/T$  is the spacing between consecutive subcarriers, and  $T_g < T$  is the duration of the cyclic prefix [2]. The structure of an OFDM transmitter is illustrated in Fig. 1. An efficient all-digital OFDM implementation is obtained by means of the inverse fast Fourier transform (IFFT) [2]. Let  $\{x(n)\}_{n=0}^{N_s-1}$  be the sequence obtained by taking the  $N_s$ -point IFFT of the symbols  $\{X(k)\}_{k=0}^{K-1}$ , as follows:

$$x(n) = \sum_{k=0}^{K-1} X(k) \exp \left\{ j2\pi \frac{kn}{N_s} \right\}, \quad n \in \{0, 1, \dots, N_s - 1\}, \quad (2)$$

where  $N_s \geq K$ . A cyclic prefix is inserted between consecutive OFDM frames to prevent interframe interference at the receiver side [2]. Appending the last  $N_g = N_s T_g / T$  samples of the sequence  $\{x(n)\}_{n=0}^{N_s-1}$  at the beginning of the sequence itself [2], we obtain the complete CP-OFDM word  $\{x(n)\}_{n=-N_g}^{N_s-1}$ .

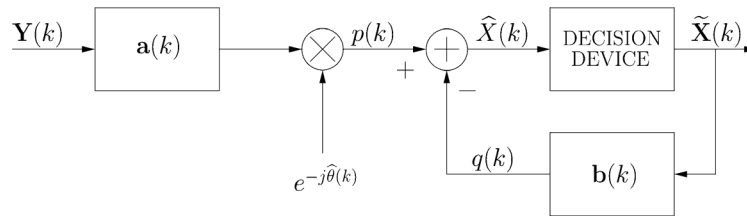


Fig. 3. Block diagram of the FD-DFE with explicit phase compensation (see the main text for definitions and notation details).

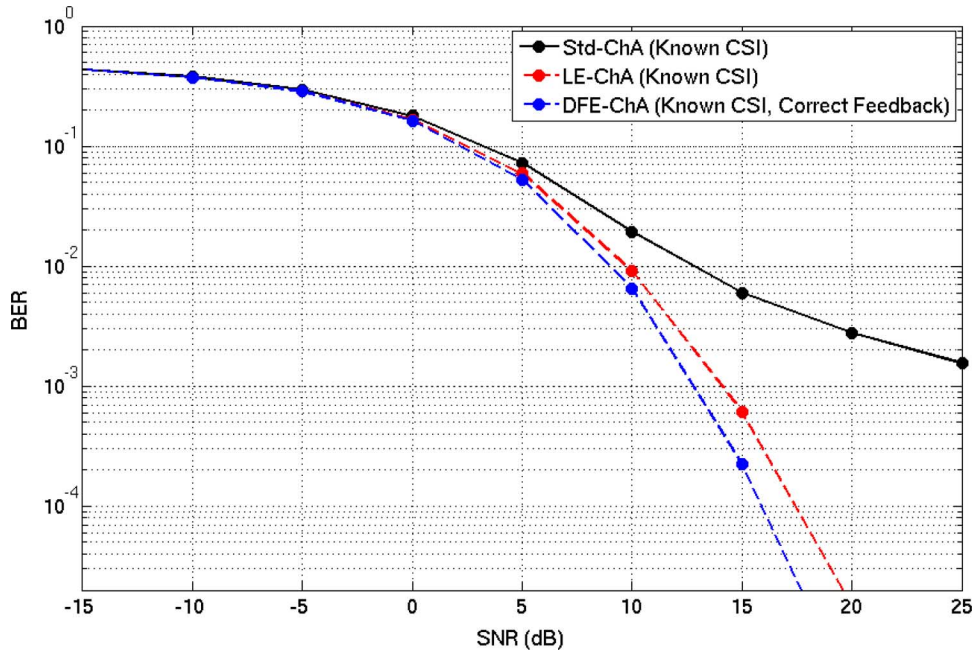


Fig. 4. Performance comparison between a receiver that neglects the ICI and the considered ICI-mitigation techniques for the time-varying channel A.

As shown in Fig. 1, the lowpass signal is then modulated onto the desired carrier frequency  $f_0$ , and the waveform  $s(t)$  that finally feeds the acoustic transducer is generated by means of a digital-to-analog converter (DAC).

The block diagram of the considered receiver is depicted in Fig. 2. The very first block is an analog-to-digital converter (ADC), which, after proper anti-aliasing filtering, samples the continuous-time signal with period  $T_s = T/N_s$ , producing the sequence  $u(n)$ . In the following, we briefly review the blocks that precede the detection block, which is the main target of our work and is discussed in Section III.

The first impairment that the considered receiver tries to mitigate is the Doppler effect due to the relative speed between the transmitter and the receiver, which is quantified by the Doppler rate  $a$ , i.e., the ratio between that speed and the speed of sound in water. We will consider wideband UWA signals, for which the Doppler effect causes, besides a frequency shift, a significant frequency spread [5]. Once a coarse estimate  $\hat{a}$  of the Doppler rate  $a$  is obtained, the received signal is resampled with period  $T_s/(1+\hat{a})$ , producing the sequence  $v(n)$ —see [5] for details on this stage. We point out that the described strategy, though based on the assumption that all propagation paths are characterized by the same time-invariant Doppler rate, is still useful when this assumption does not hold completely, since all path-dependent mismatches with respect to the estimated Doppler rate can be

considered as residual impairments to be handled in the detection stage. This point will be studied in detail for the case of the data collected in the KAM08 experiment.

After the resampling stage, the receiver works in the complex-envelope domain, defined with respect to the frequency  $f_0$ . We will denote by  $z(n)$  the complex-envelope sequence corresponding to the real-valued sequence  $v(n)$ . The next processing stage at the receiver side is aimed at achieving time synchronization, that is, at finding which samples in  $z(n)$  correspond to the transmitted sequence  $x(n)$ . Also, frequency synchronization is to be achieved, because of possible clock frequency errors/jitters, and possible uncompensated Doppler shifts. For instance, an estimation error in the Doppler rate on the order of  $10^{-4}$ , which is typical in most scenarios [5], produces a frequency offset of 1.6 Hz for a subcarrier centered at 16 kHz, which is significant for OFDM with subcarrier separation of a few Hz, as in the KAM08 experiment, and should thus be compensated. We adopt the joint time-frequency synchronization scheme proposed in [24], which exploits the presence of a cyclic prefix and, yet originally designed for frequency-flat channels, is known to be very effective also over channels with multipath propagation.

The sequence  $\{y(n)\}_{n=-N_g}^{N_s-1}$  at the output of the time-frequency synchronization block contains samples related to both the cyclic prefix and the actual OFDM data. At this stage, the

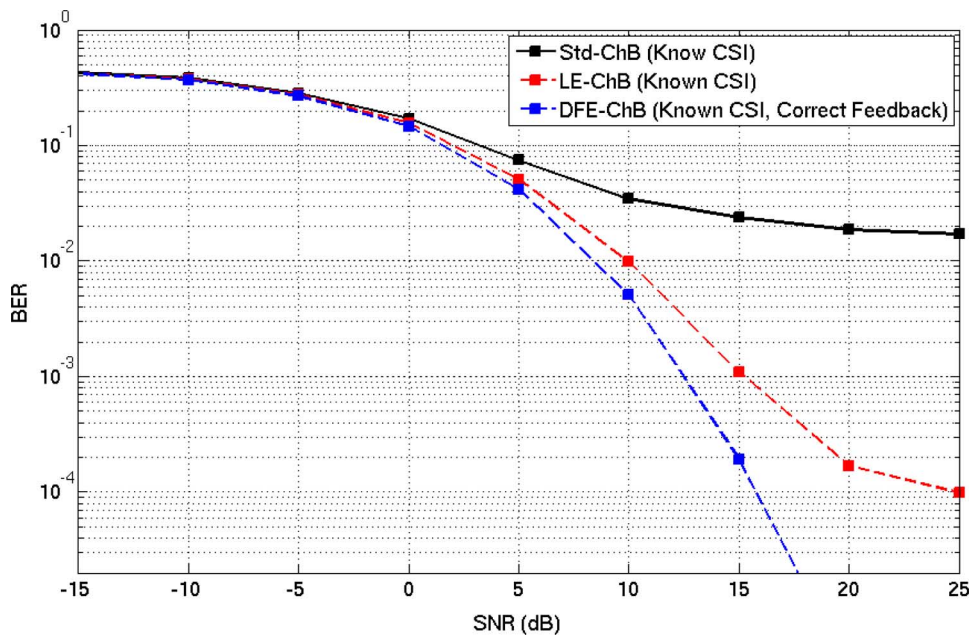


Fig. 5. Performance comparison between a receiver that neglects the ICI and the considered ICI-mitigation techniques for the time-varying channel B.

samples corresponding to the cyclic prefix are no longer useful and can be discarded. A very general discrete-time channel model is given by

$$y(n) = \sum_{\ell=0}^L c(n; \ell)x(n - \ell) + \eta(n) \quad (3)$$

where  $c(n; \ell)$  is the time-varying channel impulse response (CIR) and  $\eta(n)$  is additive white Gaussian noise (AWGN). The considered model defines the class of all linear, causal, time-varying channels of delay order  $L$ , observed in AWGN. Note that  $c(n; \ell)$  describes the explicit time variations in the CIR, but also includes the uncompensated synchronization parameters. The samples  $\{y(n)\}_{n=0}^{N_s-1}$  are processed by a fast Fourier transform (FFT)-based demodulator [2], which generates the samples

$$Y(k) = \frac{1}{N_s} \sum_{n=0}^{N_s-1} y(n) \exp \left\{ -j2\pi \frac{nk}{N_s} \right\}.$$

The relevant channel model can be written as

$$Y(k) = \sum_{m=0}^{K-1} C(k; m)X(m) + N(k) \quad (4)$$

which is of interest for  $k \in \{0, 1, \dots, K-1\}$ , that is, only for subcarrier indices at which symbols were actually transmitted. In (4),  $N(k)$  is AWGN and

$$C(k; m) = \frac{1}{N_s} \sum_{n=0}^{N_s-1} \sum_{\ell=0}^L c(n; \ell) \times \exp \left\{ j2\pi \frac{n(m-k) - m\ell}{N_s} \right\}. \quad (5)$$

The reported formulations are correct under the assumption that the duration of the cyclic prefix is at least equal to that of the CIR, that is,  $N_g \geq L$ . In the case of time-invariant channels, that is, when  $c(n; \ell)$  does not depend on the time index  $n$ , the coefficients  $C(k; m)$  are non-zero only for  $k = m$ , so that the model (4) simplifies to

$$Y(k) = C(k; k)X(k) + N(k). \quad (6)$$

In practice, provided that the cyclic prefix is long enough, the orthogonality of the subcarriers is maintained even after propagation over a time-dispersive channel, which is the key motivation for the success of OFDM systems [2]. In this paper, we address a more general scenario in which ICI arises due to significant time variations in the channel. The correct channel model is then given by (4). Comparing (4) and (6), we see that the coefficient  $C(k; m)$  describes the ICI due to the  $m$ th subcarrier on the  $k$ th subcarrier. In the following, we will often refer to the ICI coefficients using the notation “ICI coefficient with index  $i$ ”, where  $i$  is the difference between the indices of the interfering subcarriers. For example, the ICI coefficient with index 1 ( $-1$ ) describes the ICI due to the closest higher (lower) subcarrier.

### III. CHANNEL ESTIMATION AND DATA DETECTION

In this section, different approaches for channel estimation and data detection are described. All of them operate on the samples at the output of the FFT-based demodulator, which are described by the model (4).

#### A. Standard Receiver Neglecting ICI

The standard approach for OFDM detection consists of neglecting the ICI and assuming the model (6) instead of the model (4). This assumption reduces the channel estimation to the evaluation of the  $K$  complex-valued coefficients  $C(k; k)$ .

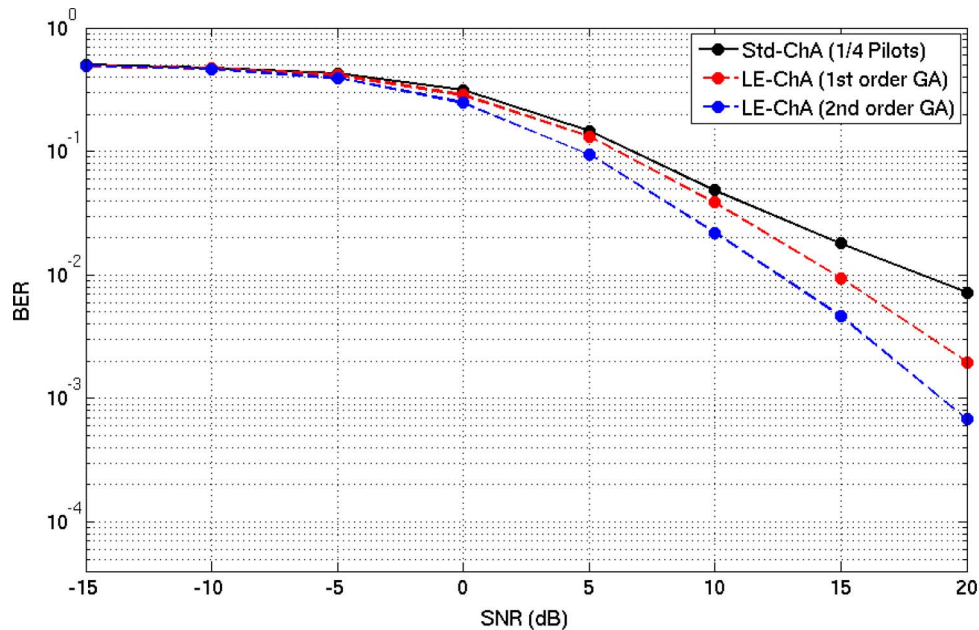


Fig. 6. Performance of FD-LE with and without the PLL in the presence of a timing offset.

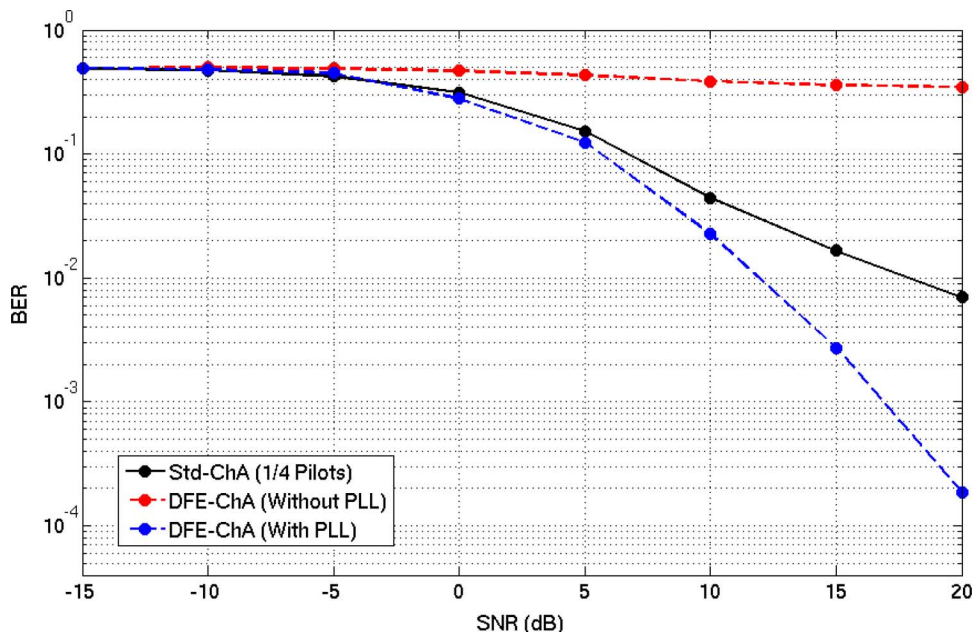


Fig. 7. Performance of FD-DFE with and without the PLL in the presence of a timing offset.

Typically, a subset of the subcarriers is reserved for pilot symbols, which are used at the receiver side for channel estimation. Although the optimal placement of the pilot symbols depends on the frequency characteristics of the channel, for simplicity the pilots are usually equally spaced. A simple interpolation-based estimation method is reviewed in the following (see [5], [25], [26], for more advanced methods). For all values of  $k$  such that  $X(k)$  is a pilot symbol, the coefficient  $C(k; k)$  is estimated as  $\hat{C}(k; k) = Y(k)/X(k)$ . Then, the remaining coefficients  $\hat{C}(k; k)$  are evaluated by linear interpolation—more advanced interpolation techniques are discussed in [25], [26]. Finally, the obtained estimates are assumed to be correct and standard coherent detection of the information symbols is carried out.

### B. ICI-Mitigation Schemes

In this section, we review the state-of-the-art solutions for ICI mitigation and motivate our choice of focusing in the rest of the paper on two specific algorithms, which are presented in the next two sections.

To mitigate Doppler-induced ICI, most recent works exploit the BEM, which allows a compact representation of the time variations in each propagation path [15]–[18]. With this model, possibly in conjunction with pulse shaping and receiver windowing [27], a sparse band representation of the frequency-domain channel matrix can be achieved. Therefore, block equalization algorithms such as those presented in [15]–[17] can be implemented with relatively low complexity. The most critical

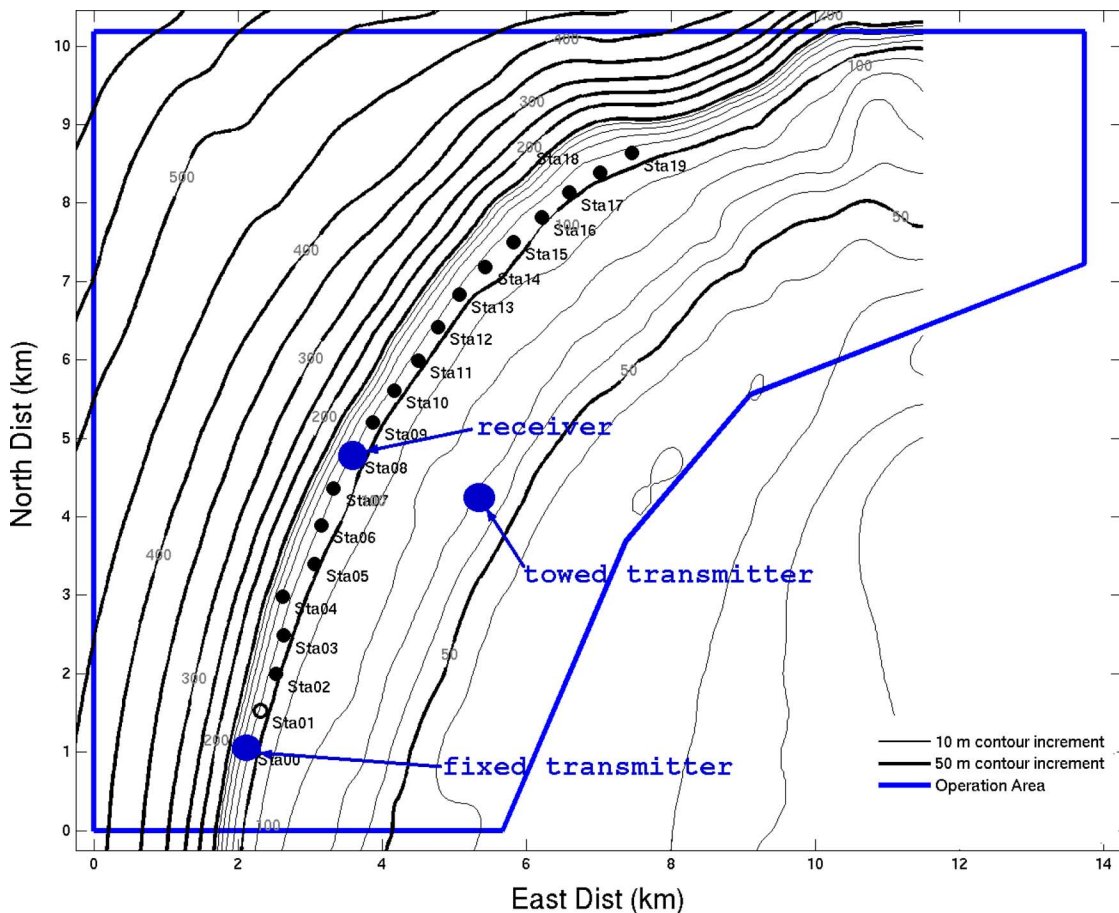


Fig. 8. Bathymetry of the operation area, with depth in meters (taken from [23]).

point in such approaches is the estimation of the BEM parameters [12]. Some recent works have shown that significant improvements can be achieved by applying the turbo principle, i.e., by iteratively improving the quality of the channel estimate based on the preliminary (soft) decisions made by the decoder [14].

When the channel spread is on the order of tens of milliseconds or more, a major drawback of most BEM-based approaches is that they do not exploit the time-domain sparseness of the UWA channel [1], thus requiring the estimation of a huge set of BEM coefficients [12]. Consequently, the ICI-mitigation ability is greatly compromised by the estimation errors, to the point that the BEM-based approaches may be even inferior to the ICI-neglecting receivers, as shown in [19]. A significant exception is given by the approach presented in [18], where by tracking the active taps of the channel impulse response the number of BEM parameters to estimate is significantly reduced. However, the underlying assumptions on the WSSUS nature of the channel and on the uniform power delay multipath profile are likely to be violated in many practical UWA scenarios. Additionally, the BEM-based approaches typically do not account for the wide-band nature of the UWA signals. Hence, a significant model mismatch arises even in the presence of a common phenomenon like the Doppler-induced time variations, which causes a frequency spreading that cannot be described by narrowband models.

Alternative ICI-mitigation approaches can be found in [19]–[21], where a specific source of ICI is addressed, i.e., the path-dependent Doppler rate. Yet very effective in such scenarios, these solutions cannot be adopted when the main source of ICI has a different form.

In the following, we consider two ICI-mitigation techniques that do not rely on any particular assumption on the channel statistics, nor on the nature of the main source of ICI. A “blind equalization” strategy is considered also in [28], where the focus is on LSQR equalizers for pulse-shape OFDM systems. The two approaches considered here are based on the application in the frequency domain of MMSE linear equalization and DFE [22], respectively. As discussed in the next sections, we enhance these standard equalization techniques by introducing a phase-tracking loop that can cope with the linear phase variations characterizing the ICI coefficients.

### C. First Approach to ICI Mitigation

A natural extension of the approximation in (6) consists of including in the channel model the ICI due to the two closest subcarriers, as follows [8], [27], [28]

$$Y(k) = \sum_{m=-1}^1 C(k; k+m)X(k+m) + N(k). \quad (7)$$

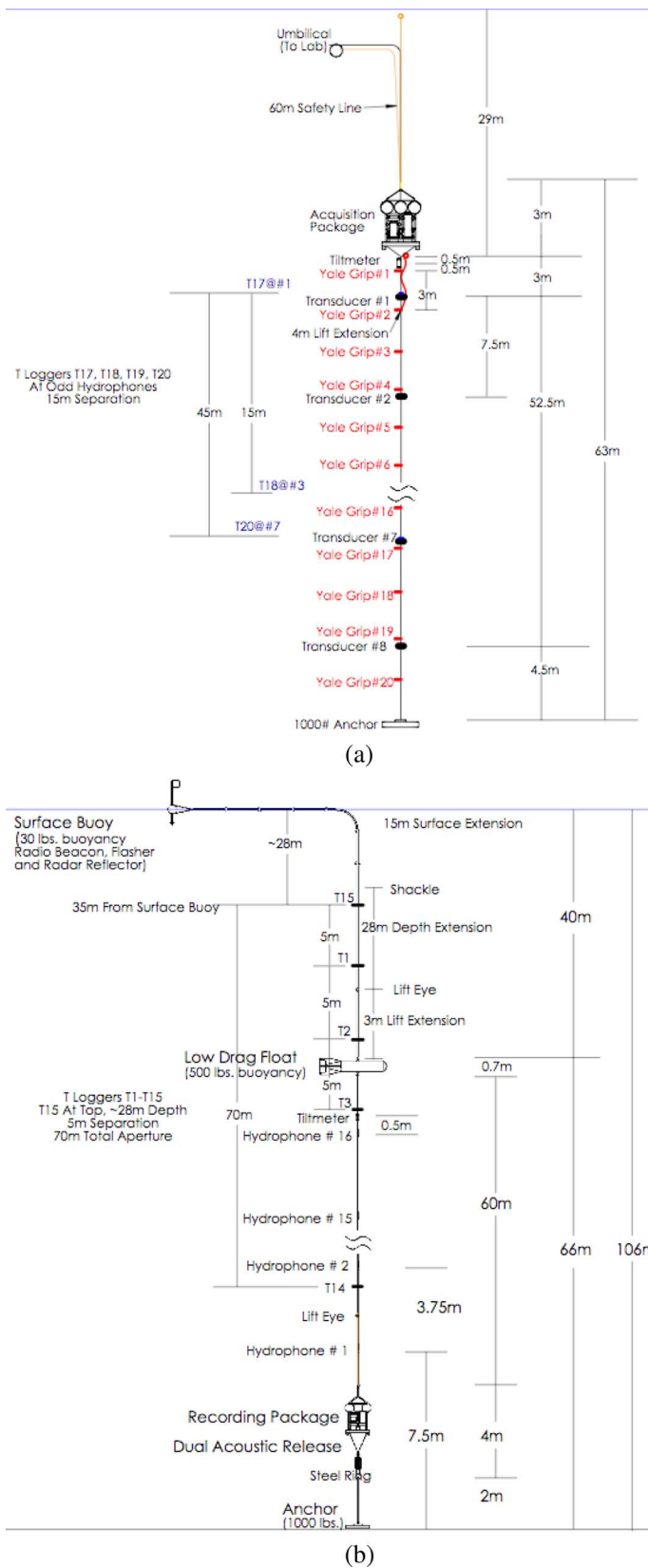


Fig. 9. Scheme of the vertical-array transmitter and receiver adopted in the KAM08 experiment (taken from [23]).

The assumption motivating the approximation of (4) by (7) is that the ICI between two subcarriers becomes weaker as their separation increases. Note that the number of channel coefficients to be estimated is now  $3K$ , instead of  $K$  as in the standard approach described earlier. Although the indices in (7) are over frequency rather than over time, the model is formally identical to the well-known problem of single-carrier transmissions affected by time-varying intersymbol interference [22]. In such scenarios, an effective way to estimate the channel coefficients is given by closed-loop tracking based on the gradient algorithm (see [29] and references therein). In our case, the application of the gradient algorithm leads to the closed-loop estimation system described in the following. Let  $\hat{C}(k; k+m)$  be the estimate of  $C(k; k+m)$ , for  $m \in \{0, \pm 1\}$ , and let us define the “error term”

$$\hat{E}(k) = Y(k) - \sum_{m=-1}^1 \hat{C}(k, k+m)X(k+m)$$

where, as a first step, we assume that all symbols  $X(k)$  are known. The channel coefficients at the subcarrier index  $k+1$  are estimated as:<sup>1</sup>

$$\hat{C}(k+1; k+1) = \hat{C}(k; k) + \gamma_0 \hat{E}(k)X(k)^*, \quad (8)$$

$$\hat{C}(k+1; k) = \hat{C}(k; k-1) + \gamma_{-1} \hat{E}(k)X(k-1)^*, \quad (9)$$

$$\hat{C}(k+1; k+2) = \hat{C}(k; k+1) + \gamma_1 \hat{E}(k)X(k+1)^* \quad (10)$$

where  $\gamma_0$ ,  $\gamma_{-1}$ , and  $\gamma_1$  are the step sizes of the closed-loop update rules, to be numerically optimized [29]. Whenever time synchronization is not perfect, the channel coefficients are affected by a phase offset that increases linearly with the index  $k$  [24]. It is then appropriate to account for such linear phase variations through the gradient algorithm. In this case, as shown in [29], the only modification to the estimation system is that the first-order loops (8), (9), and (10) become second-order loops [29].

The condition that all symbols  $X(k)$  are known pilots is clearly not of interest for communication systems. Several approaches to manage unknown symbols in closed-loop estimation systems are discussed in [29]. Here, we adopt the decision-directed mode, using the preliminary decisions made by the ICI-neglecting receiver described in Section III-A as pilots for the channel estimator. The channel estimates then feed the equalizer, which performs MMSE linear equalization (LE), as in [7]. Note that it is possible to apply the same principle iteratively, feeding the channel estimation loops with improved preliminary decisions at each iteration. This option has been studied in [14] for a different equalizer, where the benefits of iterating with an outer decoder were also investigated. With the understanding that the iterative approach can be exploited in the considered equalizer as well, for simplicity, in the following we

<sup>1</sup>The reported equations hold for PSK modulation alphabets. The formulations are more complicated for alphabets including symbols with different magnitude.

will focus on the single-iteration case, which is adopted unless otherwise specified. The approach described in this section will be briefly referred to as frequency-domain (FD) LE (FD-LE).

#### D. Second Approach to ICI Mitigation

Let us now consider an ICI-mitigation scheme that, unlike the previous one, does not rely on an explicit estimation of the ICI coefficients. The idea is to exploit the equivalence between the model (4) and the channel model for single-carrier transmissions impaired by intersymbol interference, and extend adaptive-equalization concepts developed for such scenarios to our system. Particularly, we will consider the decision-feedback equalization (DFE) technique [22], introducing an additional second-order phase tracker able to cope with the already-mentioned phase offset due to imperfect time synchronization. This structure, which will be briefly referred to as frequency-domain DFE (FD-DFE), is the frequency-domain counterpart of the time-domain approach described in [30]. We point out that no assumption on the number of significant ICI coefficients is required, unlike in (7), since the coefficients are not explicitly estimated.

Fig. 3 shows a conceptual diagram of the equalizer. Denoting by  $k$  the index of the subcarrier, the feed-forward filter  $\mathbf{a}(k)$  processes the samples  $\mathbf{Y}(k)$ , combining them and derotating the filter output, yielding to  $p(k) = \mathbf{a}'(k)\mathbf{Y}(k)e^{-j\hat{\theta}(k)}$ .<sup>2</sup> In parallel, the feedback filter  $\mathbf{b}(k)$  exploits the previously-made decisions  $\tilde{\mathbf{X}}(k)$  to compute  $q(k) = \mathbf{b}'(k)\tilde{\mathbf{X}}(k)$ , producing the term  $\tilde{X}(k) = p(k) - q(k)$  as an estimate of the transmitted symbol  $X(k)$ . An error signal  $e(k)$  is then computed as the difference between the estimate  $\tilde{X}(k)$  and the desired symbol value  $d(k)$ , which could either be the transmitted symbol  $X(k)$  for those subcarriers reserved as pilots, or the preliminary decisions  $\tilde{X}(k)$  for the remaining subcarriers. An optimization procedure is hence jointly run over the equalizer parameters  $\{\mathbf{a}(k), \mathbf{b}(k), \hat{\theta}(k)\}$ , such that the mean squared error (MSE)  $E[|e(k)|^2]$  is minimized, which requires the solution of the well-known Wiener filtering problem. To solve it, we adopt the recursive least square (RLS) procedure commonly used in the literature (see [22]).

In a similar way, we can pursue the MSE solution for the subcarrier phase offset  $\hat{\theta}(k)$ . The recursion describing  $\hat{\theta}(k)$ , according to a second-order gradient algorithm [29], can be written as

$$\hat{\theta}(k+1) = \hat{\theta}(k) + G_1 \Phi(k) + G_2 \sum_{i=0}^k \Phi(i) \quad (11)$$

where  $G_1$  and  $G_2$  are the step sizes of the loop, to be numerically optimized, and the gradient estimate  $\Phi(i)$  is computed as

$$\Phi(i) = \text{Im}\{p(i)(p(i) + e(i))^*\} = \text{Im}\{p(i)e(i)^*\}. \quad (12)$$

As for the FD-LE, the FD-DFE is initialized with preliminary decisions made according to the approach described in

<sup>2</sup>Column vectors are written in lower-case bold fonts, and the symbol  $(\cdot)'$  denotes conjugate transpose.

Section III-A and only one iteration of the equalizer is executed unless otherwise specified (see the discussion at the end of Section III-C).

#### IV. NUMERICAL RESULTS

To verify the effectiveness of the considered schemes, we present numerical results for simulated channels as well as for real data from the KAM08 experiment. Particularly, for the KAM08 experiment, both fixed- and towed-source scenarios are considered, the receiver being fixed in both cases.

##### A. Results for Simulated Channels

Our first goal is to obtain insights, through computer simulations, on the performance of different detection schemes when fast channel variations occur. The channel is simulated according to the model (3), with  $L = 10$ . The channel coefficients are obtained by independently generating each of the  $L + 1$  taps according to an exponential power delay profile [31], the last tap having, on average, half the power of the first tap. Time variations are then obtained by perturbing the resulting coefficients by means of a zero-mean Gaussian random walk with tunable variance. We consider two channels, named channel A and channel B, which differ in the variance of the random walk. Namely, the ratio between the variance of the random walk and the expected power of the first tap is  $10^{-4}$  for channel A and  $2 \cdot 10^{-4}$  for channel B, so that the variations in channel B are faster. We remark that the simulated model, which is clearly not appropriate for most UWA channels, is used only with the aim of obtaining insights on how ICI affects the system performance. The importance of such insights will be clear when the actual experimental results are discussed, later in this section.

We consider an OFDM system with uncoded BPSK transmissions, first assuming that the receiver is perfectly synchronized in time, frequency, and Doppler rate. In this ideal scenario, perfect channel-state information (CSI) is also available and, for the FD-DFE, the preliminary decisions fed back are correct. Figs. 4 and 5 compare the performance of the considered detection schemes in terms of bit-error rate (BER) versus signal-to-noise ratio (SNR), for the case  $K = 2048$ ,  $N_s = 12800$ ,  $N_g = 1000$ , and three-tap filters for both equalizers. Considering (3), we define the SNR as

$$\text{SNR} = \frac{E[|x(n)|^2]}{E[|\eta(n)|^2]} \sum_{\ell=0}^L E[|c(n; \ell)|^2]$$

where  $E[\cdot]$  denotes statistical expectation. Note that, in both simulated scenarios, BER floors are unavoidable when ICI is neglected, while they can be effectively mitigated when ICI-mitigation techniques are adopted. We also notice that, while both techniques are effective, the FD-DFE outperforms the FD-LE in both channels, the improvement becoming more noticeable as the time variations increase. Note that, at low values of the SNR, the performance of the classical approach is basically the same as that of the receivers with ICI mitigation. Hence, the simulations suggest that, given the statistics of the channel variations, two different regimes can be distinguished based on the SNR.

In the former regime, which will be referred to as noise-limited, the ICI power is much lower than the noise power, so that no significant performance improvement can be achieved by ICI mitigation; in the latter, which will be referred to as ICI-limited, the ICI power is on the order of (or greater than) the noise power, so that the detection performance is remarkably improved by ICI mitigation.

We now investigate the performance of the same system when the assumptions of ideal CSI and error-free preliminary decisions are removed, and the detection algorithms work in the adaptive mode described in Section III exploiting the pilot symbols placed every four tones. Also, aimed at verifying the robustness of the considered approaches to synchronization errors, we assume that an error of 90 samples affects the detection of the start-of-CP sample—note that the error corresponds to less than 10% of the CP duration (i.e.,  $N_g = 1000$ ). As discussed in Section III, the timing error causes a linear phase rotation of the frequency-domain channel coefficients, which motivated our choice of adopting a phase tracking loop in the ICI-mitigation receivers. The need for this solution is proved by the simulation results reported in Figs. 6 and 7, which both refer to channel A. Interestingly, while the FD-DFE exhibits a huge performance degradation in the absence of the phase-locked loop (PLL), the FD-LE is fairly robust to phase rotations even if a first-order gradient algorithm (GA) is adopted. This is due to the fact that the FD-DFE, utilizing a RLS-based algorithm, is effective only when the channel to equalize is stationary [22]. This condition clearly does not hold in presence of carrier phase rotations. On the contrary, for the FD-LE, there is no such strict constraint imposed, and therefore the absence of the second-order GA only results in a gradient estimate offset, proportional to the amount of phase rotations [29]. In our example, this offset is relatively small with respect to the actual value of the gradient.

##### B. Results for the KAM08 Experiment—Fixed-Source Scenario

Our experimental data were collected during the KAM08 experiment [23], which was conducted in shallow water off the western coast of Kauai, HI, in June 2008. The bathymetry of the operation area is shown in Fig. 8. We present results for a fixed-source scenario and for a towed-source scenario (the relevant details are given later). The positions of the adopted transmitters and receivers are shown in Fig. 8.

Let us start from the fixed-source scenario, where no intentional motion between the transmitter and the receiver is present, and the resampling stage can thus be avoided. An 8-element vertical-array source was deployed with an interelement separation of 7.5 m and an aperture of 52.5 m. The top element was at a nominal depth of 30 m, and the bottom element was not anchored to the sea floor. As receiver, a 16-element vertical array was deployed, at a distance of 4 km from the source. The sampling rate was 50 kHz. The inter-element spacing was 3.75 m, with the top element deployed at a nominal depth of 42.25 m. A pictorial description of the adopted vertical arrays is given in Fig. 9.

Our first purpose is to verify the presence of non-negligible ICI in the experimental data. To do this, we estimate the ICI power by exploiting a probe OFDM signal, operating in the band spanning from 12.5 to 25 kHz. The signal incorporates 2048

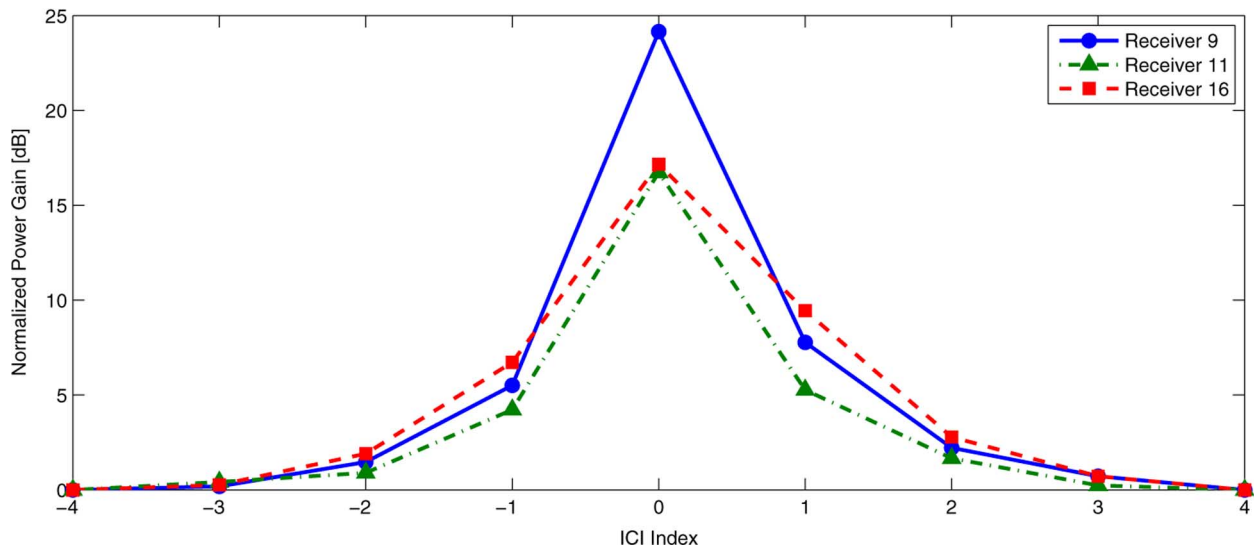


Fig. 10. Estimates of the average power of the main tap (ICI index 0) and various ICI coefficients.

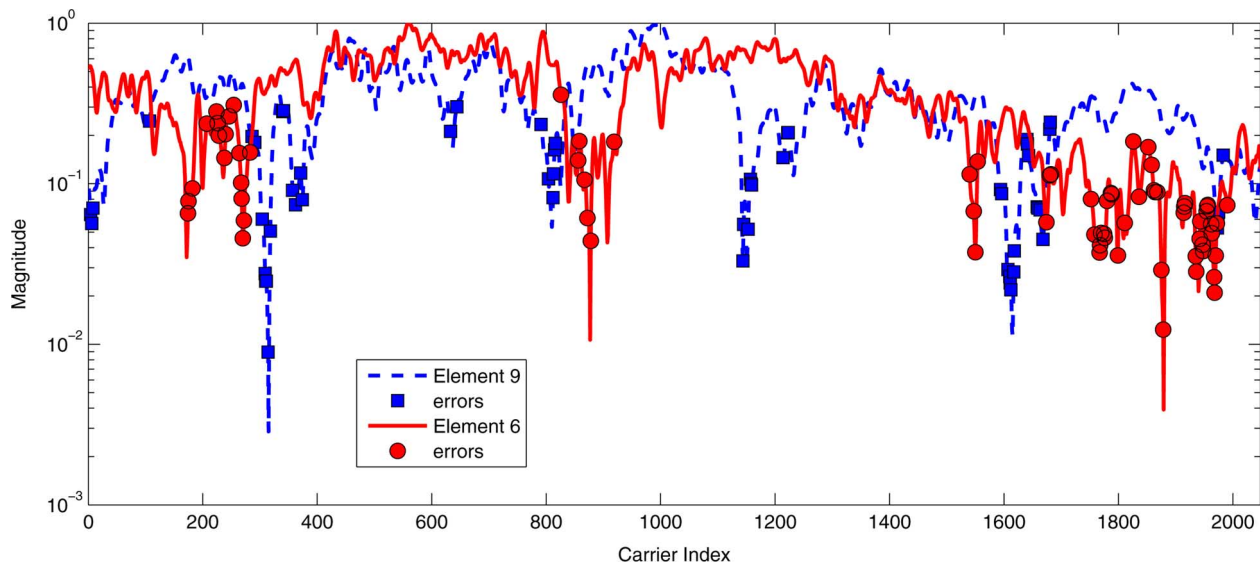


Fig. 11. Estimated magnitude of the channel gain and positions of the decoding errors for two different receiving elements.

subcarriers, with a subcarrier spacing of 6.1 Hz, a frame length of 164 ms, and a silence interval of 100 ms between two consecutive frames—since the channel delay spread was estimated to be on the order of 10 ms [32], interframe interference can be safely neglected. The OFDM signal was structured such that only one of every eight carriers was modulated with a BPSK symbol, while all other carriers were not used. According to (4), under the reasonable assumption that the ICI between subcarriers with a separation of at least eight positions is negligible, each sample  $Y(k)$  can be rewritten as

$$Y(k) = C(k, \hat{m})X(\hat{m}) + N(k) \quad (13)$$

where  $\hat{m}$  is the index of the non-silent subcarrier closest to  $k$ . Hence, according to (13), the power of the sample  $Y(k)$  provides a (noisy) estimate of the power of  $C(k, \hat{m})$ , since the

BPSK symbols are such that  $|X(\hat{m})| = 1$ . Fig. 10 shows the average power of the estimated ICI coefficients for three different elements in the receiver array, in the case of transmissions from element 8 (that is, the deepest one, at a depth of 82.5 m) in the source array. At the receiver side, elements 9, 11, and 16 were at depths of 68.5, 61, and 42.25 m, respectively. As expected, the average ICI power decreases as the magnitude of the ICI index increases. Note that, on average, the ICI power from the two closest carriers (ICI index  $\pm 1$ ) is much lower than that of the main tap (ICI index 0), but significantly greater than that of the weakest ICI coefficients and that of the noise. Particularly, we point out that the ICI power from the two closest carriers is, on average, from 4 to 9 dB greater than the noise power, depending on the receiver considered, which suggests that the ICI should be accounted for in the receiver design. Also, Fig. 10 shows that the assumption of neglecting the ICI between non-consecutive carriers, as we did in the derivation of the FD-LE technique, is a good approximation.

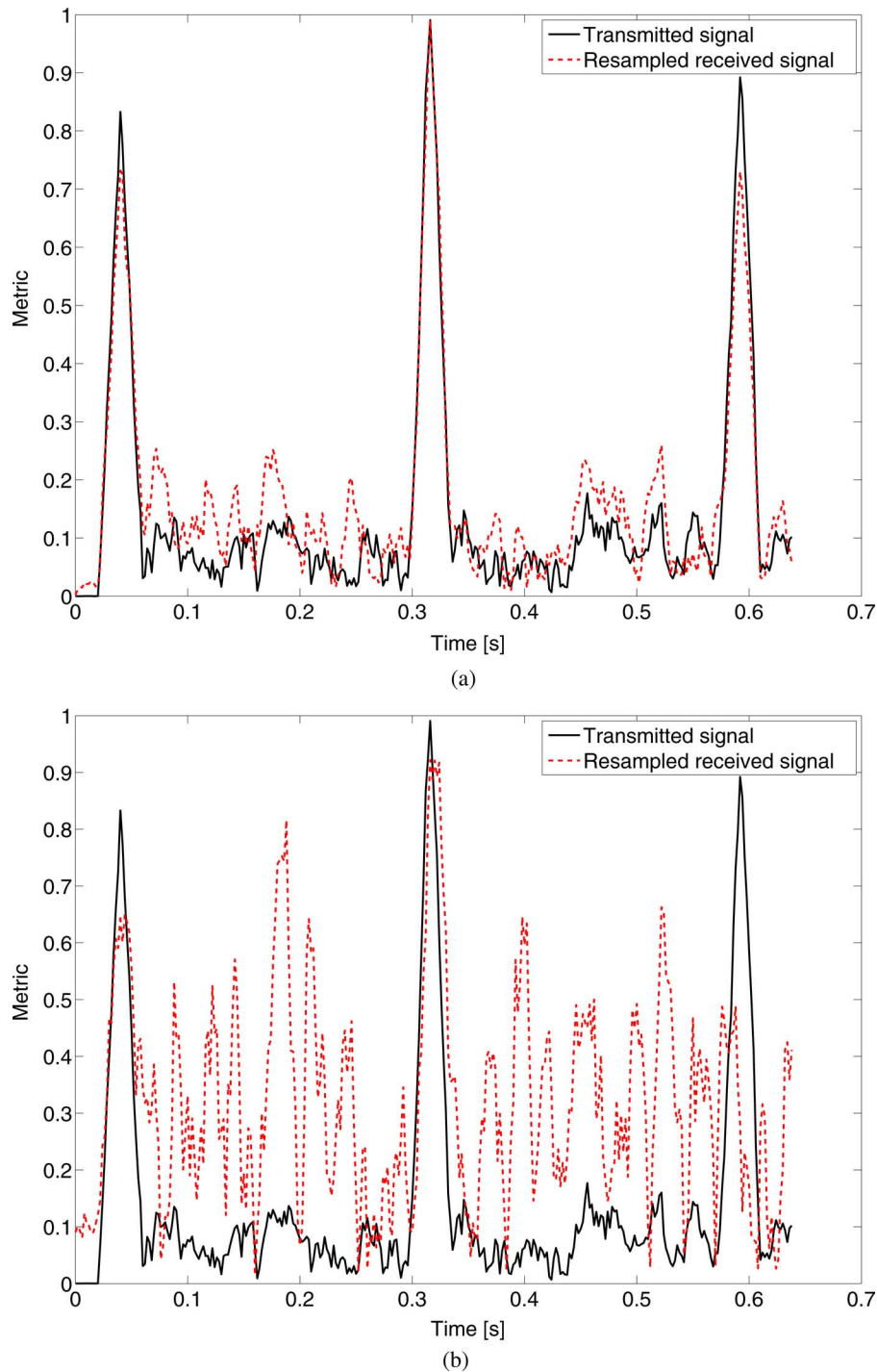


Fig. 12. Comparison of different time synchronization metrics. (a) Resampling with  $\hat{a} = 1.14 \cdot 10^{-3}$ . (b) Resampling with  $\hat{a} = 1.67 \cdot 10^{-3}$ .

TABLE I  
UNCODED BER IN THE FIXED-SOURCE SCENARIO

Receiving elements	Standard	FD-LE	FD-DFE
9	5.2%	4.3%	4.5%
16	12.1%	10.0%	10.8%
9 and 16 (MRC)	2.2%	1.4%	1.5%

Let us now consider communication data collected in the same experiment. We first focus on the results for a 2048-carrier OFDM system adopting a BPSK modulation. The signal

has a frequency band spanning from 12 to 20 kHz and a cyclic prefix of 20 ms, which implies a word duration of 276 ms. In each OFDM word, one symbol every four is used as a pilot symbol, and 36 symbols are reserved for peak-to-average power ratio (PAPR) reduction purposes, so that there are 1500 information bits. An example of the performance of different detection schemes is reported in Table I, for the case of transmissions from element 8 and reception at elements 9 and 16. We considered single-element processing as well as multielement processing with maximal-ratio combining (MRC). The reported results are

TABLE II  
UNCODED BER IN THE TOWED-SOURCE SCENARIO WHEN ICI IS NEGLECTED

$\hat{a} \cdot 10^3$	1.18	1.14	1.11	1.05	1.02	1.00
With Frequency Synchronization	2.9%	2.9%	2.9%	3.1%	3.1%	50.0%
No Frequency Synchronization	3.1%	3.0%	3.1%	14.9%	26.1%	36.3%

obtained by averaging the uncoded BER over 12 000 information bits transmitted in a few consecutive seconds. The parameters of the equalizers have been optimized for each OFDM word, which led to the following values: one-tap filters,  $\gamma_i \in [0.06, 0.15]$ ,  $G_1 \in [0.25, 1.2]$ , and  $G_2 \in [0.00025, 0.012]$ . Similar results were obtained by processing data recorded at different times during the experiment, and considering different elements both at the transmitter and the receiver side. According to the terminology of Section IV-A, this scenario is noise-limited, particularly when the receiving element 9 is considered: the performance improvement provided by ICI mitigation is relatively limited. The fact that the scenario is noise-limited might seem in contrast with the estimates in Fig. 10, which show that the power of the ICI due to the closest carriers is, on average, much greater than the noise power. Insights into this fact are given by the results reported in Fig. 11, where the estimated magnitude of the main coefficient (ICI index 0) is shown, together with the positions of the decoding errors for the FD-DFE technique. It is clear that the errors occur mostly where the channel has spectral notches, that is, where the system is very likely to be noise-limited, which is not in contrast with the estimates in Fig. 10, since the latter quantities are averages over the entire spectrum.

Finally, we point out that the BERs obtained in all considered scenarios are on the order of 2%–20% when only one receiving element is exploited, but it is possible to obtain BERs on the order of 1% (or lower) by combining the outputs of different receiving elements, that is, by exploiting the fact that the spectral notches occur at different frequencies for different elements (see Fig. 11). Particularly, by means of MRC over three elements, we are able to correctly detect all information bits in more than 95% of the processed frames. A very similar performance, i.e., no errors over 90% of the processed frames, is obtained also with QPSK-modulated signals, again by combining 3 receiving elements. In every considered scenario, the uncoded BER is well below the value that can be corrected by means of modern rate-1/2 channel codes. Hence, when such codes are used, we can confidently expect a BER on the order of  $10^{-4}$  or less.

### C. Results for the KAM08 Experiment—Towed-Source Scenario

We now consider the experimental data collected in the presence of motion between the transmitter and the receiver. Namely, the transmitter was submerged at a depth spanning from 20 to 50 m, depending on the specific experiment, and towed at a nominal speed of 3 knots (i.e., about 1.54 m/s), while the receiver was the same 16-element array described in Section IV-B. Particularly, we consider the case when the link

range was approximately 2 km, and the towing ship was moving towards the fixed receiver, with the transmitting transducer about 25 m below the sea surface. Unlike for the fixed-source experiment, no probe OFDM signal was transmitted. All reported results refer to communication signals adopting BPSK modulation, with the same OFDM format and pilot allocation as described in Section IV-B.

If the received signal is processed without the resampling stage, the information sequence cannot be recovered (a BER of 50% is observed). It is thus necessary to estimate the Doppler rate and to resample the received sequence accordingly. A coarse estimate of the Doppler rate can be obtained by exploiting the synchronization signals that were periodically inserted between OFDM words in the KAM08 experiment to facilitate Doppler-rate estimation. In this case, the estimate of the Doppler rate is  $\hat{a} = 1.14 \cdot 10^{-3}$ , which is consistent with the actual status of the moving ship, since the value of  $\hat{a}$  corresponds to a speed of about 1.7 m/s towards the receiver, i.e., very close to the nominal speed of the towing ship. In the following, we show how the estimate  $\hat{a}$  impacts the performance of the various receiver blocks.

Let us start with the time synchronization algorithm, which immediately follows the resampling stage. We consider the time synchronization metric proposed in [24], implemented in the pure-correlation form. Fig. 12 shows the time synchronization metric obtained after resampling the signal received at element 5 with  $\hat{a} = 1.14 \cdot 10^{-3}$  (top figure) and  $\hat{a} = 1.67 \cdot 10^{-3}$  (bottom figure), both compared with the synchronization metric characterizing the transmitted signal, which is the metric obtained at the output of the transmitter and exhibits clear peaks every 276 ms (i.e., the duration of the OFDM word). Note that the metric obtained after resampling with  $\hat{a} = 1.14 \cdot 10^{-3}$  closely resembles the metric characterizing the transmitted signal, thus yielding an effective time synchronization. On the other hand, Fig. 12 shows that, after resampling with  $\hat{a} = 1.67 \cdot 10^{-3}$ , the metric is completely distorted and proper time synchronization cannot be achieved, which implies that no information can be recovered at the receiver side. By means of similar analyses, we could conclude that an accuracy of at least  $5 \cdot 10^{-4}$  in the estimate of the Doppler rate is required for the time synchronization to work effectively.

Next, we evaluate how the estimate  $\hat{a}$  affects the frequency synchronization stage. Table II compares the uncoded BER performance of the standard receiver that neglects the ICI, with and without the frequency synchronization stage of the signal received at element 5. Note that, when no frequency synchronization is performed, the accuracy of the Doppler rate estimation is very critical for the BER performance, while it is not critical when frequency synchronization is performed, for a wide

TABLE III  
UNCODED BER IN THE TOWED-SOURCE SCENARIO FOR DIFFERENT DETECTION ALGORITHMS

$\Delta a \cdot 10^3$	0.00	0.14	0.16	0.19	0.21	0.23	0.25
Standard Approach	0.3%	35.7%	43.1%	50.0%	50.0%	50.0%	50.0%
FD-LE	0.1%	4.5%	4.0%	3.3%	2.8%	3.2%	4.1%
FD-DFE	0.1%	0.7%	0.7%	0.9%	1.1%	1.1%	1.2%

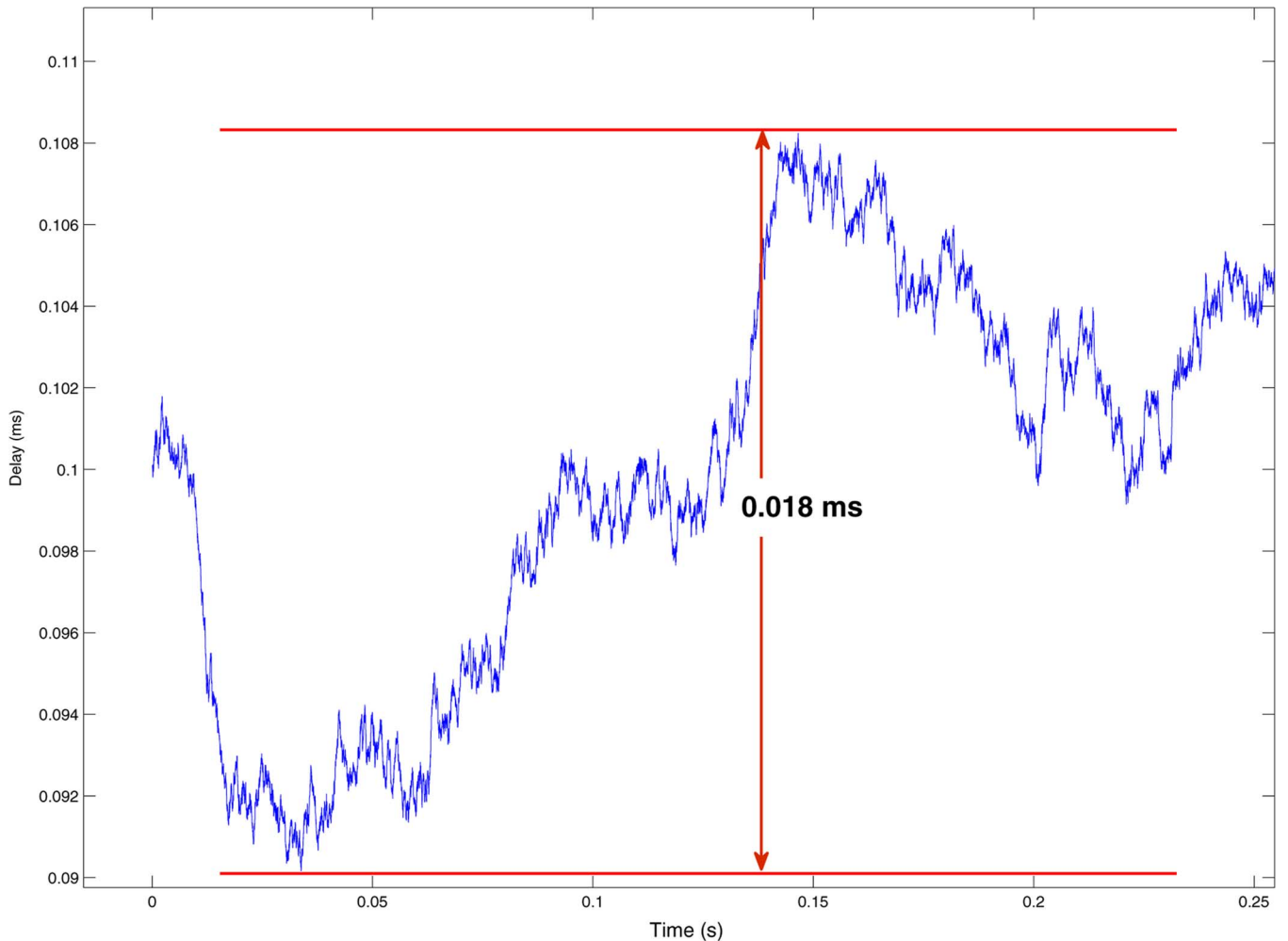


Fig. 13. A realization of the process  $\Lambda(n)$  with  $\sigma_\epsilon = 0.005$ .

range of values of  $\hat{a}$ . These (and other) results suggest that, provided that the accuracy in the estimation of the Doppler rate is on the order of  $1.4 \cdot 10^{-4}$  or less, the residual Doppler shift after resampling can be effectively compensated for by the frequency synchronization algorithm. However, when the residual Doppler shift is such that the resulting frequency offset does not belong to the acquisition range of the frequency synchronization algorithm, the ICI-neglecting receiver completely fails (see the entry  $\hat{a} = 10^{-3}$  in Table II). Interestingly, as shown in Table III for the case of MRC of element 5, 8, and 16, the robustness to the residual Doppler shift can be greatly improved if ICI mitigation is adopted, again with FD-DFE outperforming FD-LE. In this case, the first run of both FD equalizers is effectively driven only by the pilot symbols, since the preliminary

decisions obtained by standard detection are basically random (see the entry “Standard Approach” in Table III). Hence, it is useful to execute multiple iterations of the equalizer, using as preliminary decisions the equalizer output at the previous iteration. The results shown in Table III refer to the case of six iterations for both ICI-mitigation schemes. The other parameters are:  $\gamma_i \in [0.06, 0.09]$ ,  $G_1 \in [0.8, 2.95]$ ,  $G_2 \in [0.007, 0.0011]$ , and three-tap filters. Note that the optimized number of taps for the equalization filters is greater than in the fixed-source scenario, which is consistent with the observation that the ICI is more pronounced in the towed-source scenario. Note that the improvements provided by ICI mitigation are consistent with the fact that, ultimately, the effect of a residual Doppler shift is ICI [21].

TABLE IV  
UNCODED BER FOR THE INTENTIONALLY DEGRADED EXPERIMENTAL DATA

$\sigma_e \cdot 10^3$	Standard Approach	FD-LE	FD-DFE
15.0	16.1%	13.6%	1.0%
10.0	7.3%	7.1%	0.5%
5.0	1.2%	0.9%	0.2%

After evaluating the impact of the accuracy in the Doppler rate estimation, we finally discuss the detection performance obtained when the actual estimate  $\hat{\alpha} = 1.14 \cdot 10^{-3}$  is adopted in the resampling stage. In this case, after proper compensation of the Doppler shift, most of the data collected in the KAM08 experiment seem to correspond to noise-limited scenarios, for which ICI mitigation does not provide a remarkable performance improvement with respect to the standard receivers. This fact suggests that, compared to the duration of the OFDM words, the channel variations were relatively slow in that environment. It is interesting to evaluate how such conclusions would change in a more challenging UWA environment, with faster time variations. A simple procedure that allows us to introduce artificial time variations in the experimental data consists of resampling the received signal with time-varying rate. Formally, the sequence is resampled so that, for the  $n$ th sample, the difference between the nominal sampling time  $nT_s$  and the actual sampling time is  $\Lambda(n)$ . Note that the obtained sequence is basically equivalent to a sequence obtained with ideal sampling rate when the multipath propagation is characterized by the time-varying delay  $\Lambda(n)$ . We here consider  $\Lambda(n)$  generated according to a zero-mean Gaussian random walk with standard deviation  $\sigma_e \cdot T_s$ ,  $\sigma_e$  being a tunable parameter. A realization of the process  $\Lambda(n)$  with  $\sigma_e = 0.005$  is shown in Fig. 13. Note that, within an observation window of 250 ms (i.e., roughly the duration of the considered OFDM word), the variations of  $\Lambda(n)$  are on the order of the nominal sampling interval  $T_s = 20 \mu\text{s}$ . Interestingly, this value corresponds to a variation of about 2 cm in the length of the propagation paths, which seems to be a realistic variation in 250 ms, for many practical UWA environments. Average values of the uncoded BER obtained by processing the resampled sequences are reported in Table IV for three different values of  $\sigma_e$  and three different detection algorithms with MRC of elements 5, 8, and 16. The results refer to the case of three iterations for both ICI-mitigation schemes. The other parameters are:  $\gamma_i \in [0.06, 0.2]$ ,  $G_1 = 0.8$ ,  $G_2 = 0.007$ , and three-tap filters. Note that the FD-LE does not provide a significant performance improvement with respect to the ICI-neglecting receiver, which shows that the effectiveness of the FD-LE is greatly compromised when the estimation of the ICI coefficients is critical. On the other hand, the FD-DFE is very robust to time-varying propagation delays, and emerges as a promising solution for UWA channels with more challenging time variations than those characterizing the data collected in the KAM08 experiment.

## V. CONCLUSION

We have considered OFDM transmissions over time-varying UWA channels, comparing the performance of standard receivers

neglecting ICI with that achievable by means of two ICI-mitigation schemes. In the first scheme, the ICI coefficients are explicitly estimated by means of a closed-loop tracking system, and FD-LE equalization based on such estimates is performed. In the second scheme, detection is performed by means of an adaptive FD-DFE, which does not require explicit ICI estimation. Simulation results show that in ICI-limited scenarios both techniques provide a significant performance improvement with respect to the standard OFDM receivers, typically with FD-DFE being more effective than FD-LE. Receivers employing ICI mitigation outperform the standard ones in the decoding of real UWA data from the recent KAM08 experiment, particularly when scenarios with motion between the transmitter and the receiver are considered. In these cases, ICI mitigation significantly increases the robustness of the receiver to imperfect compensation of the motion-induced Doppler shift. Finally, we have shown the potential of the ICI-mitigation schemes in coping with more challenging time variations than those characterizing the environment of the KAM08 experiment. These results serve as an encouragement to investigate related decision-feedback structures, such as those that exploit both forward and backward directions for adaptive detection of symbols in an OFDM block.

## REFERENCES

- [1] M. Stojanovic, "Underwater acoustic communications: Design considerations on the physical layer," in *Proc. Wireless on Demand Network Syst. Serv.*, Jan. 2008, pp. 1–10.
- [2] J. A. C. Bingham, "Multicarrier modulation for data transmission: An idea whose time has come," *Electron. Lett.*, vol. 28, pp. 5–14, May 1990.
- [3] E. Bejjani and J. C. Belfiore, "Multicarrier coherent communications for the underwater acoustic channel," in *Proc. IEEE Oceans 1996*, Sep. 1996, pp. 1125–1130.
- [4] M. Stojanovic, "Low complexity OFDM detector for underwater acoustic channels," in *Proc. IEEE Oceans 1996*, Boston, MA, Sept. 2006, pp. 1–6.
- [5] B. Li, S. Zhou, M. Stojanovic, L. Freitag, and P. Willett, "Multicarrier communication over underwater acoustic channels with nonuniform Doppler shifts," *IEEE J. Oceanic Eng.*, vol. 33, no. 2, pp. 198–209, Apr. 2008.
- [6] Y. Emre, V. Kandasamy, T. M. Duman, P. Hursky, and S. Roy, "Multi-input multi-output OFDM for shallow-water UWA communications," in *Proc. Acoust.*, Jun. 2008, pp. 13–17.
- [7] T. Wang, J. G. Proakis, and J. R. Zeidler, "Techniques for suppression of intercarrier interference in OFDM systems," in *Proc. IEEE Wireless Commun. Netw. Conf.*, Mar. 2005.
- [8] L. Rugini, P. Banelli, and G. Leus, "Simple equalization of time-varying channels for OFDM," *IEEE Commun. Lett.*, pp. 619–621, Jul. 2005.
- [9] X. Huang and H. Wu, "Robust and efficient intercarrier interference mitigation for OFDM systems in time-varying fading channels," *IEEE Trans. Veh. Technol.*, vol. 56, no. 5, pp. 2517–2528, Sep. 2007.

- [10] A. F. Molisch, M. Toeltsch, and S. Vermani, "Iterative methods for cancellation of intercarrier interference in OFDM systems," *IEEE Trans. Veh. Technol.*, vol. 56, no. 4, pp. 2158–2167, Jul. 2007.
- [11] L. Zou, Q. Chang, C. Xiu, and Q. Zhang, "Channel estimation and ICI cancellation for OFDM systems in fast time-varying environments," *IEICE Trans. Commun.*, vol. E91-B, no. 4, pp. 1203–1206, Apr. 2008.
- [12] Z. Tang, R. C. Cannizzaro, G. Leus, and P. Banelli, "Pilot-assisted time-varying channel estimation for OFDM systems," *IEEE Trans. Signal Processing*, vol. 55, no. 5, pp. 2226–2238, May 2007.
- [13] C. Tepedelenlioglu and G. B. Giannakis, "Blind estimation and equalization of time- and frequency-selective channels using filterbank precoders," in *Proc. 32nd Asilomar Conf. Signals, Syst., Comput.*, Pacific Grove, CA, Nov. 1998, pp. 1138–1142.
- [14] K. Fang, L. Rugini, and G. Leus, "Iterative channel estimation and turbo equalization for time-varying OFDM systems," in *Proc. IEEE Int. Conf. Acoust., Speech Signal Processing (ICASSP 2008)*, Las Vegas, NV, Mar. 2008, pp. 2909–2912.
- [15] K. Fang *et al.*, "Low-complexity block turbo equalization for OFDM systems in time-varying channels," *IEEE Trans. Signal Processing*, vol. 56, no. 11, pp. 5555–5566, Nov. 2008.
- [16] L. Rugini, P. Banelli, and G. Leus, "Low-complexity banded equalizers for OFDM systems in Doppler spread channels," *EURASIP J. Appl. Signal Processing*, vol. 2006, pp. 1–13, 2006, Article ID 67404.
- [17] P. Schniter, "Low-complexity equalization of OFDM in doubly selective channels," *IEEE Trans. Signal Processing*, vol. 52, no. 4, pp. 1002–1011, Apr. 2004.
- [18] S. J. Hwang and P. Schniter, "Efficient multicarrier communication for highly spread underwater acoustic channels," *IEEE J. Sel. Areas Commun.*, vol. 26, no. 9, pp. 1674–1683, Dec. 2008.
- [19] S. Mason, C. R. Berger, S. Zhou, K. R. Ball, L. Freitag, and P. Willett, "Receiver comparisons on an OFDM design for Doppler spread channels," in *Proc. MTS/IEEE Oceans*, Bremen, Germany, May 2009.
- [20] C. R. Berger, S. Zhou, J. Preisig, and P. Willett, "Sparse channel estimation for multicarrier underwater acoustic communication: From subspace methods to compressed sensing," *IEEE Trans. Signal Processing*, vol. 58, no. 3, pp. 1708–1721, Mar. 2010.
- [21] S. Mason, C. Berger, S. Zhou, K. Ball, L. Freitag, and P. Willett, "An OFDM design for underwater acoustic channels with Doppler spread," in *Proc. Digital Signal Processing Workshop 5th IEEE Signal Processing Education Workshop*, Jan. 2009, pp. 138–143.
- [22] J. G. Proakis, *Digital Communications*, 4th ed. : McGraw-Hill, 2001.
- [23] W. S. Hodgkiss, H. C. Song, M. Badiey, A. Song, and M. Siderius, Kauai Acomms MURI 2008 (KAM08) Experiment—Trip Report Tech. Rep., Jul. 2008.
- [24] J. J. van de Beek, M. Sandell, and P. O. Borjesson, "ML estimation of time and frequency offset in OFDM systems," *IEEE Trans. Signal Processing*, vol. 45, no. 7, pp. 1800–1805, July 1997.
- [25] S. Coleri, M. Ergen, A. Puri, and A. Bahai, "Channel estimation techniques based on pilot arrangement in OFDM systems," *IEEE Trans. Broadcast.*, vol. 48, no. 3, pp. 223–229, 2002.
- [26] M. Hsieh and C. Wei, "Channel estimation for OFDM systems based on comb-type pilot arrangement in frequency selective fading channels," *IEEE Trans. Consumer Electron.*, vol. 44, no. 1, pp. 217–225, 1998.
- [27] S. Das and P. Schniter, "Max-SINR ISI/ICI-shaping multicarrier communication over the doubly dispersive channel," *IEEE Trans. Signal Processing*, vol. 55, no. 12, pp. 5782–5795, Dec. 2007.
- [28] M. Hampejs, P. Svac, G. Tauböck, K. Gröchenig, F. Hlawatsch, and G. Matz, "Sequential LSQR-based ICI equalization and decision-feedback ISI cancellation in pulse-shaped multicarrier systems," in *Proc. IEEE SPAWC 2009*, Perugia, Italy, June 2009.
- [29] U. Mengali and A. N. D. Andrea, *Synchronization Techniques for Digital Receivers*. New York: Plenum, 1997.
- [30] M. Stojanovic, J. Catipovic, and J. G. Proakis, "Phase coherent digital communications for underwater acoustic channels," *IEEE J. Oceanic Eng.*, vol. 19, no. 1, pp. 100–111, 1994.
- [31] A. Goldsmith, *Wireless Communications*, 2nd ed. Cambridge, U.K.: Cambridge University Press, 2005.
- [32] A. Radosevic, J. Proakis, and M. Stojanovic, "Statistical characterization and capacity of Shallow water acoustic channels," in *Proc. IEEE Oceans 2009*, Bremen, Germany, May 2008.

**Kai Tu** received the B.S. degree (with honors) in electrical engineering from the East China Normal University, Shanghai, China, in 1999 and the M.S. degree in electrical engineering from the Arizona State University (ASU), Tempe, in 2008.

From 1999 to 20004, he was a Consultant and Application Engineer at the Shanghai Representative Office of Nicolet Instrument Technologies, Inc., Madison, WI. In August 2004, he was admitted to the M.S. program of the Department of Electrical Engineering at ASU, where he conducted research on speech codec, adaptive beamforming and sound localization algorithms. In August 2005, he transferred to the Arts, Media and Engineering program of the same department, to work on particle filtering for sound location, and probabilistic models in the context of mediated active learning. In January 2008, he joined the Wireless Communications Lab at ASU, where he is currently working towards the Ph.D. degree. His research interest is in adaptive equalization, interference cancellation, Doppler mitigation, and capacity analysis of time-varying multipath channels, mostly in the context of MIMO-OFDM underwater acoustic communications.

**Dario Fertonani** was born in Mantua, Italy, in 1980. He received the M.S. degree in telecommunications engineering in 2004 and the Ph.D. degree in information technology in 2008, both from the University of Parma, Parma, Italy.

He held a postdoctorate position at Arizona State University, Tempe, from May 2008 to December 2009. Currently, he works at Qualcomm, Inc., San Diego, CA. His research interests include various topics in digital communications and information theory, with a particular focus on detection and coding for channels with memory. He is the coauthor of several publications in international journals and conferences.

**Tolga M. Duman** (F'11) received the B.S. degree from Bilkent University, Turkey in 1993, and the M.S. and Ph.D. degrees from Northeastern University, Boston, MA, in 1995 and 1998, respectively, all in electrical engineering.

Currently, he is a Professor of Electrical Engineering with the School of Electrical, Computer and Energy Engineering at Arizona State University, Tempe. Since August 1998, he has been with the Electrical Engineering Department of Arizona State University, first as an Assistant Professor (1998–2004), then as an Associate Professor (2004–2008), and starting August 2008 as a Professor. His current research interests are in systems, with particular focus on communication and signal processing, including wireless and mobile communications, coding/modulation, coding for wireless communications, data storage systems, and underwater acoustic communications.

Dr. Duman has served as an Editor for IEEE TRANSACTIONS ON WIRELESS COMMUNICATIONS (2003–08) and IEEE ONLINE JOURNAL OF SURVEYS AND TUTORIALS (2002–2007). He is currently an Editor for IEEE TRANSACTIONS ON COMMUNICATIONS in the area of coding and communication theory (2007–present), and for Elsevier *Physical Communications Journal* (2010–present). Dr. Duman is a Fellow of IEEE, a recipient of the National Science Foundation CAREER Award, and IEEE Third Millennium medal.

**Milica Stojanovic** (SM'08–F'10) graduated from the University of Belgrade, Serbia, in 1988, and received the M.S. and Ph.D. degrees in electrical engineering from Northeastern University, Boston, MA, in 1991 and 1993, respectively.

After a number of years with the Massachusetts Institute of Technology (MIT), Cambridge, where she was a Principal Scientist, she joined the faculty of Electrical and Computer Engineering Department at Northeastern University in 2008. She is also a Guest Investigator at the Woods Hole Oceanographic Institution, MA, and a Visiting Scientist at MIT. Her research interests include digital communications theory, statistical signal processing and wireless networks, and their applications to underwater acoustic communication systems.

Dr. Stojanovic is an Associate Editor for the IEEE JOURNAL OF OCEANIC ENGINEERING and the IEEE TRANSACTIONS ON SIGNAL PROCESSING.

**John G. Proakis** (S'58–M'62–SM'82–F'84–LF'97) received the B.S.E.E. degree from the University of Cincinnati, OH, in 1959, the M.S.E.E. degree from the Massachusetts Institute of Technology (MIT), Cambridge, in 1961, and the Ph.D. degree from Harvard University, Cambridge, MA, in 1967.

He is an Adjunct Professor at the University of California at San Diego and a Professor Emeritus at Northeastern University, Boston, MA. He was a faculty member at Northeastern University from 1969 through 1998 and held the following academic positions: Associate Professor of Electrical Engineering, 1969–1976; Professor of Electrical Engineering, 1976–1998; Associate Dean of

the College of Engineering and Director of the Graduate School of Engineering, 1982–1984; Interim Dean of the College of Engineering, 1992–1993; Chairman of the Department of Electrical and Computer Engineering, 1984–1997. Prior to joining Northeastern University, he worked at GTE Laboratories and the MIT Lincoln Laboratory. His professional experience and interests are in the general areas of digital communications and digital signal processing. He is the coauthor of the books *Digital Communications* (New York: McGraw-Hill, 2008, fifth edition), *Introduction to Digital Signal Processing* (Upper Saddle River: Prentice Hall, 2007, fourth edition); *Digital Signal Processing Laboratory* (Englewood Cliffs: Prentice Hall, 1991); *Advanced Digital Signal Processing* (New York: Macmillan, 1992); *Algorithms for Statistical Signal Processing* (Upper Saddle River: Prentice Hall, 2002); *Discrete-Time Processing of Speech Signals* (New York: Macmillan, 1992, IEEE Press, 2000); *Communication Systems Engineering*, (Upper Saddle River: Prentice Hall, 2002, second edition); *Digital Signal Processing Using MATLAB V.4* (Boston: Brooks/Cole-Thomson Learning, 2007, second edition); *Contemporary Communication Systems Using MATLAB* (Boston: Brooks/Cole-Thomson Learning, 2004, second edition); *Fundamentals of Communication Systems* (Upper Saddle River: Prentice Hall, 2005).

**Paul Hursky** (S'97–M'08) received the B.S. and M.S. degrees in physics from the University of Pennsylvania, Philadelphia, in 1978 and 1980 and the Ph.D. degree in electrical engineering from the University of California at San Diego in 2001.

From 1980 to 1999, he was with Lockheed Aeronautical Systems Company, Burbank and San Diego, CA, where he worked on signal processing algorithm development for sonar systems. From 1999 to 2004, he was with Science Applications International, Inc., where he worked on advanced concepts for underwater acoustic applications. From 2004 to the present, he has been with Heat, Light, and Sound Research, Inc., a company he helped to start, where he works on research topics in underwater acoustics, including acoustic propagation modeling, model-based signal processing, marine mammal tracking, and acoustic communications.

Dr. Hursky is a member of the IEEE Signal Processing, Ocean Engineering, Communications, and Information Theory Societies, and the Acoustical Society of America.